AIAA JOURNAL
Vol. 45, No. 11, November 2007

Noise and Spreading of Subsonic Coannular Jets—Comparison with Single Equivalent Jet

K. B. M. Q. Zaman* and M. D. Dahl†
NASA John H. Glenn Research Center at Lewis Field, Cleveland, Ohio 44135

DOI: 10.2514/1.29441

The issue of scaling of noise as well as spreading of subsonic coannular jets is revisited. Far-field noise and centerline pitot-static pressure surveys are conducted with concentric, circular nozzles having an outer–to–inner diameter ratio of 1.42. Both the inner nozzle and the outer annular passage are convergent. Outer–to–inner Mach number ratio R is varied over a large range from 0 to about 10. Results are examined on the basis of single equivalent jet parameters calculated by satisfying continuity, momentum, and energy equations. The results confirm that coannular jets with "normal" velocity profiles are noisier than the equivalent jet. Jets with "inverted" velocity profiles are also found to be noisier except in the R range of 1–1.5. There, a few cases exhibit lower intensities (by a fraction of a dB) relative to the intensity at $R = 1$. However, other run conditions exhibit the lowest intensity at $R = 1$. Thus, the present data with unheated flow and the given nozzle geometry do not clearly exhibit noise reduction with the inverted velocity profile jets. For the flowfield, the asymptotic Mach number decay rates as well as the potential core lengths are found to be comparable to those of the equivalent jet.

Nomenclature

A	=	cross-sectional area
D	=	nozzle diameter
M	=	Mach number at nozzle exit
p	=	static pressure
p'	=	rms pressure fluctuation
R	=	Mach number ratio, M_2/M_1
r	=	microphone distance from nozzle exit
T	=	total temperature
t	=	static temperature
U	=	streamwise velocity
x	=	streamwise distance from nozzle exit
θ	=	angular location of microphone relative to downstream jet axis

Subscripts

a	=	ambient
eq	=	equivalent
j	=	jet at nozzle exit
m	=	mixed
o	=	outer nozzle
1	=	inner stream at nozzle exit
2	=	outer annular stream at nozzle exit

I. Introduction

THIS study was prompted by earlier investigations of noise reduction with offset (eccentric) coannular nozzles [1,2]. The reduction of noise was measured relative to that of the corresponding concentric configuration. For the latter basic configuration, some questions came up regarding the scaling of the noise vis-à-vis that of a "single equivalent jet." These are addressed in this paper with the help of experimental data from a concentric coannular nozzle having convergent inner as well as outer annular flows.

For a given primary jet, it has been known that the onset of the outer annular flow attenuates noise when measured at a fixed microphone location [3,4]. However, thrust and mass-flow rate also change with the addition of the annular flow. Those must be accounted for to assess the net impact on the noise field relative to that of a single equivalent jet. The issue was addressed, among others, by Tanna [4]. He reached the inference that coannular jets are, in fact, noisier for normal velocity profiles (inner jet having higher velocity) but quieter for a range of conditions for inverted velocity profiles (inner jet having lower velocity).

The procedures for the determination of the SEJ (single equivalent jet) [5], however, have not been reviewed critically. In [4], a constant area condition was invoked in addition to satisfying continuity and momentum equations. That is, the exit area of the SEJ was assumed to be the same as the exit area of the outer nozzle. A detailed analysis for noise prediction was carried out in [5]; a constant area condition was also followed for obtaining the SEJ parameters for the merged flow region of the jet. In [6,7], a further comprehensive analysis was carried out for correlation and prediction of coannular jet noise. The analysis drew on experimental results of the flowfield, for example, reported in [8]. The equivalent jet was defined differently for different flow regions, to be discussed further in the text (Sec. IV.B). In [9] as well as [7], while analyzing heated jet data, enthalpy conservation was also satisfied besides continuity and momentum for obtaining the SEJ parameters. Even though the present experiment involves "cold" flow (that is, the total temperature is constant throughout and equal to that in the ambient), the data analysis is carried out on the latter basis satisfying the full set of conservation equations. The constant area procedure is also considered to examine the impact on the results.

Coannular jets are known to spread more slowly. With the addition of the annular flow the potential core of the primary jet extends farther downstream. Again, similar considerations come into play and one may ask how these characteristics, when viewed in terms of the SEJ, would compare with single jet measurements. In this investigation, we address these issues and also review the impact of various simplifications in the derivation of the SEJ parameters. The overall intensity and spectra of the far-field noise, covering a wide range of velocity ratios, are analyzed first. Jet spreading, based on centerline Mach number decay, is then examined.

Presented as Paper 0210 at the 43rd AIAA Aerospace Sciences Meeting, Reno, NV, 10–13 January 2005; received 22 December 2006; revision received 12 June 2007; accepted for publication 29 June 2007.

*Aerospace Engineer, Aerpropulsion Division, Inlet and Nozzle Branch, Mail Stop 5-12. Associate Fellow AIAA.

†Aerospace Engineer, Aeropropulsion Division, Acoustics Branch, Mail Stop 54-3. Senior Member AIAA.

II. Experimental Facility

Figure 1 shows the open jet facility in which the experiment was conducted [2]. A streamlined probe holder mounted on a traversing mechanism, for flowfield measurements, can be seen in the foreground. For noise measurements, all exposed surfaces in the vicinity of the facility were covered with sound absorbing material. The primary nozzle was attached to the 30 in. diam main plenum chamber of the facility. Another annular plenum chamber, located just upstream of the nozzles, provided the outer (secondary) flow. The outer flow, supplied by four equally spaced ports, was routed through contoured interior and screens to provide a uniform velocity profile at the exit. Flow uniformity was checked by pitot probe surveys [2]. For the present experiment, the inner nozzle was convergent with an exit diameter of 1.48 in. and a lip thickness of 0.03 in. The outer annular passage was also convergent. The diameter of the outer nozzle D_o was 2.1 in. The nozzles were essentially "coplanar" with the inner nozzle lip protruding slightly (0.125 in.) relative to the exit of the outer nozzle. The ratio of the primary–to–annular exit area was 0.92. Subsonic flow, ensuring shock-free operation in both streams, was ensured for all results presented in this paper.

Pitot-static probe surveys were conducted on the axis of the jet over the x/D_o range, −0.2–26.3. The probe had a 0.065 in. outer diameter with static ports located 0.39 in. from the tip. For $x/D_o > 5$, the measured static pressure was assumed to apply at the tip (pitot) location, for calculation of the Mach number. Close to the nozzle, because of sharper gradients, separate static pressure runs were carried out to match the locations of pitot pressure data. The axis of the probe traversing mechanism was carefully aligned with the jet axis; velocity maps on the cross-sectional plane at $x/D_o = 14$ showed that the two axes were within 0.5 deg of each other [2]. With all data (flow as well as noise), the two mass-flow rates and plenum pressures were recorded simultaneously. Since the cross-sectional area ratio was 0.92, the bypass ratio was close to R. Only R is quoted with all data presented in the following.

The far-field noise was measured with (B&K model 4135) microphones located at $37.1D_1$ and $50.2D_1$ from the nozzle exit for $\theta = 25$ deg and 90 deg, respectively. Spectral analysis of the microphone signal was done by a Nicolet 660B analyzer. The entire test chamber had sound absorbing "baffles" on the ceiling and "coatings" on the upper half of all four walls. For this experiment, the floor and other exposed surfaces in the vicinity of the facility were wrapped with sound absorbing material. Nevertheless, the picture in Fig. 1 should indicate that the environment was far from ideal for noise measurement. Thus, an assessment of the quality of the noise data was desired.

Figure 2 shows power spectral density for the primary jet only, compared to data from a few other facilities. These include a set of data from the aeropropulsion laboratory ("dome") at NASA John H. Glenn Research Center (GRC) [10], a set from UC–Irvine [1], and another one from an experiment at Boeing Seattle facilities [11]. The reference "Z&Y" stands for earlier experiments in the anechoic flow facility of NASA Langley [12]. The nozzle diameters (in inches) and jet Mach numbers are indicated in the legends; "atm-c" indicates that correction for atmospheric attenuation has been performed [13]. The sound power spectral density (PSD) is normalized as $P^* = (p'/\rho_j U_j^2)^2 (r/D)^2 (U_j/(\Delta f D))$ [12]. Here, p' is the rms pressure fluctuation in the frequency band Δf, and ρ_j, U_j, and M_j represent the density, velocity, and Mach number at the nozzle exit. (An astute reader should note that for simplicity ρ_a was substituted for ρ_j in [12].) The rationale for scaling P^* with $M_j^{5.5}$ at shallow angles (Fig. 2a) and with $M_j^{3.5}$ at 90 deg (Fig. 2b) is based on correlation of several sets of noise data available at the time of the cited investigation. The adopted scaling yielded the best collapse of the data. This implied a $U^{8.5}$ and a $U^{6.5}$ scaling for the spectral amplitudes at $\theta = 25$ deg and 90 deg, respectively.

First, let us consider the data from the other facilities in Fig. 2. The normalized PSD have collapsed reasonably. The Boeing data involve the largest nozzle and have some undulations on the low-frequency end. The UCI data are with the smallest nozzle and reflect fine quality. However, there are differences that may not be insignificant. Note that P^* involves $(p')^2$ and thus each decade on the

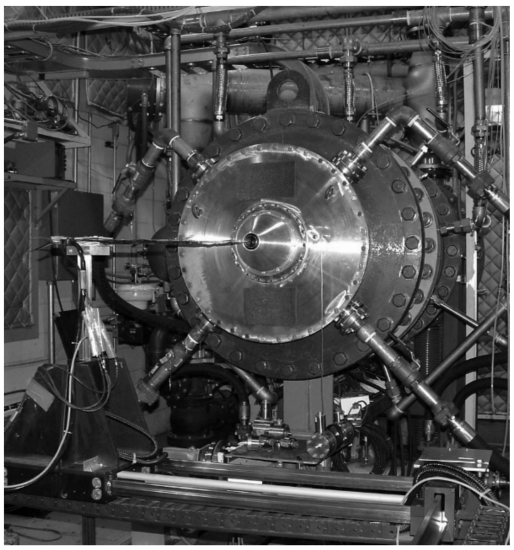

Fig. 1 Jet facility.

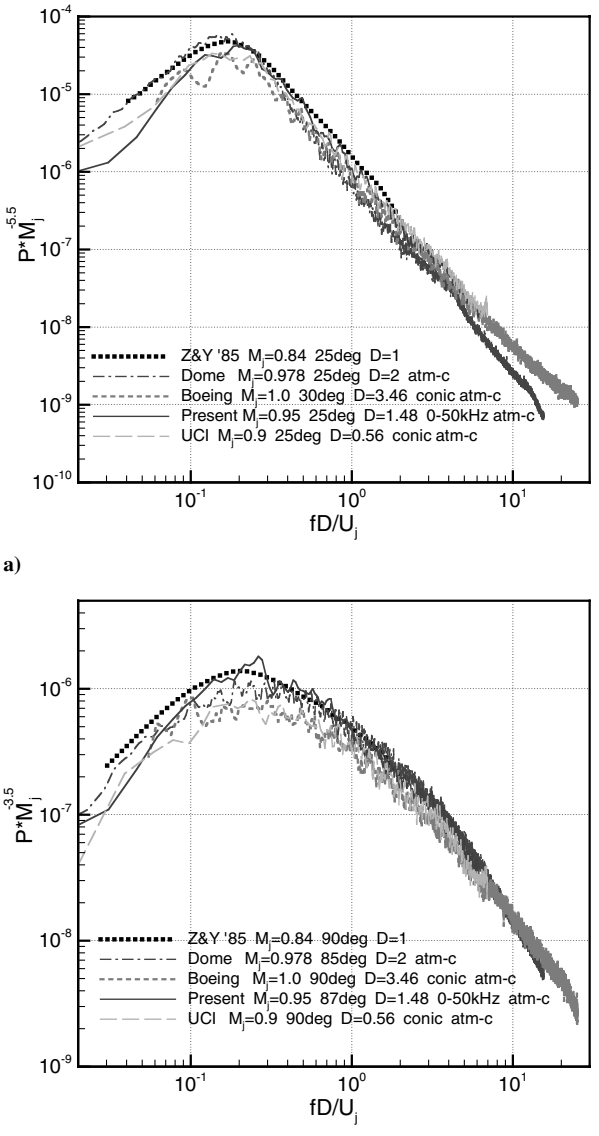

Fig. 2 Noise power spectral density compared to data from other facilities: a) $\theta = 25$ deg; b) $\theta = 90$ deg.

ordinate represents 10 dB in sound pressure level (SPL). The scatter near the spectral peak is about 1.5 dB. Away from the peak the amplitude scatter may be more. It is emphasized that "scatter" in this context refers to variations in data from different facilities and not data repeatability in a given facility. It is near impossible to identify all sources contributing to the scatter. Apart from differences in test chamber conditions and "internal noise," simply the hardware geometry can have an impact. In the Boeing experiment [11], more than 2 dB difference occurred (on the high-frequency end) with two nozzles having different internal contours [American Society of Mechanical Engineers (ASME) profile versus conic] with all other test conditions remaining the same. Data from the conic nozzle is shown in Fig. 2; the ASME nozzle was noisier. It remains unclear how nozzle geometry factors in. Besides influencing transmission of internal noise another possibility is via a difference in the exit boundary layer characteristics. In the GRC experiment, nozzle size as well as boundary layer state made a difference ([10]; see also [14]). The upshot is that about 2 dB scatter is still the reality in jet noise data quality, although this is a significant improvement since [12] when more than 5 dB scatter was noted.

Figure 2 shows that the present data fall reasonably close to this scatter band. Notable disagreements are the lower amplitude on the low-frequency end in Fig. 2a and a bump near the peak in Fig. 2b. However, the overall agreement is quite well in view of the imperfect test chamber conditions and the data quality is considered adequate for the comparative investigation at hand. All spectral data in the following are obtained with same bandwidth (0–50 kHz) and same averaging period (45 s).

III. Single Equivalent Jet Parameters

The parameters of the single equivalent jet can be found from a simplified analysis of the equations of motion. Consider an imaginary flow in which the coannular jet mixes within a short distance from the nozzle to yield a single jet. A control volume (CV) for such a flow is sketched in Fig. 3. Note that the boundary of the CV is shown to converge since the equivalent diameter would be usually smaller than the outer nozzle diameter. The streamwise extent of the domain can be very short and there is no friction, heat transfer, or entrainment. The static pressure is the same as ambient on all surfaces. Entering the CV is the coannular jet with the inner stream having a uniform velocity U_1 and the outer stream having a uniform velocity U_2. The two streams have cross-sectional areas of A_1 and A_2, respectively. Exiting the CV is a single stream with uniform velocity U_{eq} and cross-sectional area A_{eq}.

The equation for the conservation of mass in a steady flow applied over the surface of the CV can be written as $\oint_A \rho \boldsymbol{V} \circ \hat{n} dA = 0$, where $\boldsymbol{V}$ is the velocity vector, ρ is the density, and $\hat{n}$ is the outward normal vector on the surface A. Performing integration over the control surface, one obtains

$$-\rho_1 U_1 A_1 - \rho_2 U_2 A_2 + \rho_{\text{eq}} U_{\text{eq}} A_{\text{eq}} + \int_{A0} \rho \boldsymbol{V} \circ \hat{n}\, \mathrm{d}A = 0 \qquad (1)$$

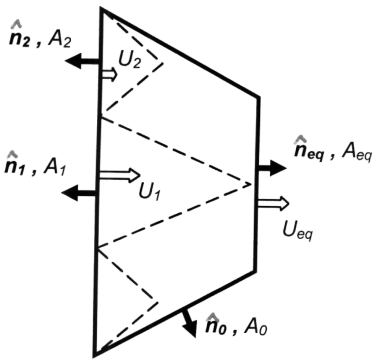

Fig. 3 Control volume for coannular jet analysis.

The last integral is zero by definition, so that

$$\rho_1 U_1 A_1 + \rho_2 U_2 A_2 = \rho_{\text{eq}} U_{\text{eq}} A_{\text{eq}} \qquad (2)$$

The integral form of the conservation of momentum over the control surface is similarly written as

$$\oint_A (\rho \boldsymbol{V}) \boldsymbol{V} \circ \hat{n}\, \mathrm{d}A + \oint_A p \hat{n}\, \mathrm{d}A = 0$$

where p is the static pressure. This is a vector equation with components in the axial and the radial directions. Here, the axial component of the momentum equation is of interest. Performing integration over the surface, one obtains

$$-\rho_1 U_1^2 A_1 - \rho_2 U_2^2 A_2 + \rho_{\text{eq}} U_{\text{eq}}^2 A_{\text{eq}} - \left(p_{\text{eq}} A_{\text{eq}} - p_1 A_1 - p_2 A_2 + \int_{A0} p\, \mathrm{d}A \right) = 0 \qquad (3)$$

Because the static pressure is the same on all surfaces, the net contribution from the pressure terms within the parentheses is zero. Thus, one obtains

$$\rho_1 U_1^2 A_1 + \rho_2 U_2^2 A_2 = \rho_{\text{eq}} U_{\text{eq}}^2 A_{\text{eq}} \qquad (4)$$

At this point, we have two equations for determining the three parameters describing the SEJ: ρ_{eq}, U_{eq}, and A_{eq}. A third equation is required. In comparing the noise levels from a coannular jet and from a single equivalent jet, Tanna [4] discusses the need to hold three parameters constant. The first two parameters held constant are the mass flow and thrust, which are expressed in Eqs. (2) and (4). For the third parameter, Tanna chooses to hold the total nozzle exit area a constant,

$$A_1 + A_2 = A_{\text{eq}} \qquad (5)$$

Another choice would be to hold the total energy a constant. Pao [9] and Fisher et al. [7] used forms of the energy equation in their analyses for the SEJ parameters. We consider this latter approach.

The integral equation over the control surface is obtained for the conservation of total energy after neglecting viscous effects, heat transfer effects, and potential energy changes.

$$\oint_A (E + p) \boldsymbol{V} \circ \hat{n}\, \mathrm{d}A = 0 \qquad (6)$$

In this equation, E is the total energy per unit volume. The process of performing the integration over the surfaces of the CV is the same as above. The resulting equation is

$$(E_1 + p_1) U_1 A_1 + (E_2 + p_2) U_2 A_2 = (E_{\text{eq}} + p_{\text{eq}}) U_{\text{eq}} A_{\text{eq}} \qquad (7)$$

Applying thermodynamic relationships and assuming constant specific heats, Eq. (7) can be rewritten as

$$T_1 \rho_1 U_1 A_1 + T_2 \rho_2 U_2 A_2 = T_{\text{eq}} \rho_{\text{eq}} U_{\text{eq}} A_{\text{eq}} \qquad (8)$$

where T is the total temperature. Equation (8) is a statement of the conservation of energy in terms of total enthalpy. However, because the total temperature is the same everywhere in the present experiment, Eq. (8) reduces to Eq. (2), thus not producing a unique relation. To obtain such a relation, we use the definition for total temperature,

$$T_a = t_{\text{eq}} + \frac{U_{\text{eq}}^2}{2C_p} = t_1 + \frac{U_1^2}{2C_p} = t_2 + \frac{U_2^2}{2C_p} \qquad (9)$$

where t is the static temperature. To relate static temperature with density we use the equation of state (with $\boldsymbol{R}$ denoting the gas constant) and noting that the static pressure is a constant,

$$p_a = \boldsymbol{\rho}_{\text{eq}} \boldsymbol{R} t_{\text{eq}} = \boldsymbol{\rho}_1 \boldsymbol{R} t_1 = \boldsymbol{\rho}_2 \boldsymbol{R} t_2 \qquad (10)$$

We are left with four unknowns, ρ_{eq}, A_{eq}, U_{eq}, and t_{eq}, that can be

solved for a given pair of driving pressures for the inner and outer flows from Eqs. (2), (4), (9), and (10).

In the following data analysis, SEJ parameters obtained by satisfying the full set of conservation equations as outlined in the foregoing will be used. This will be referred to as the "constant enthalpy" procedure. For comparison, the "constant area" procedure of Tanna will also be considered. For calculation of the SEJ parameters with the latter method, Eq. (9) is replaced by Eq. (5).

For the present nozzle geometry, the quantities D_{eq}, M_{eq}, and t_{eq} are calculated by the constant enthalpy and constant area procedures and shown in Figs. 4a–4c, respectively. The results are shown as a function of the Mach number ratio R. The parameters calculated with constant area procedure are shown by the thin line curves. Naturally, D_{eq} is a constant for this case. The equivalent Mach number is a maximum at $R = 1$ and falls off monotonically on either side. The static temperature is minimum at $R = 1$. Away from $R = 1$ on either side the temperature continues to increase.

The parameters obtained with the constant enthalpy procedure are shown by the thick line curves. One finds that D_{eq} is the maximum at $R = 1$ and decreases on either side. The limiting value of D_{eq} is D_1 at $R = 0$. It is equal to the equivalent diameter of the outer annulus at $R = \infty$. Ideally, D_{eq} should be equal to D_o at $R = 1$ but it is somewhat less due to the lip thickness of the inner nozzle. M_{eq}, on the other hand, reaches minima at about $R = 0.5$ as well as 2.5. It will be noted shortly that the overall intensity when plotted as a function of R also exhibits minima at approximately these two values of R. The static temperature now has realistic values, with maxima where M_{eq} has minima. Unless stated specifically, D_{eq} and M_{eq} obtained with the constant enthalpy procedure are used in the following. The SEJ parameters, considered in [6,7], will be discussed with the spectral data in Sec. IV.B.

IV. Results and Discussion

Sound pressure level spectra were measured for different combinations of M_1 and M_2. The overall intensities, obtained by integration of the spectra, are shown in Figs. 5a and 5b for $\theta =$ 25 deg and 90 deg, respectively. There are four sets of data: 1) $M_1 \approx 0.96$ with varying M_2, 2) $M_2 \approx 0.99$ with varying M_1, 3) $M_1 \approx 0.79$ with varying M_2, and 4) $M_2 \approx 0.72$ with varying M_1. A fifth set of data is included in Fig. 5a for $M_1 \approx 0.61$. For set 2 ($M_2 \approx 0.99$) an additional data point at large R is shown—disconnected, because the primary pressure was at the limits of the transducer range and hence the accuracy of R was poor. The case, $R = \infty$ ($M_1 = 0$) has been excluded because it appeared abnormally noisy possibly due to excitation of plenum chamber resonances. In Fig. 5a, for $R < 1$, trends as reported in [3,4] can be seen: as R increases the intensity first decreases, reaches a minimum at $R \approx 0.5$, and then increases. For $M_2 \approx$ const cases, a steep initial drop in intensity occurs with increasing R. For $R > 2.5$ the intensity increases again. Corresponding data for $\theta = 90$ deg, shown in Fig. 5b, exhibit essentially similar trends. These intensity data are analyzed on the basis of equivalent jet parameters in the following.

A. Scaling of Overall Intensity

The data of Figs. 5a and 5b are normalized by D_{eq} and M_{eq} and shown in Figs. 6a and 6b, respectively. Normalization with an equivalent diameter has been done so as to refer the data at $r/D_{eq} = 50$. Normalization with the Mach number involves a scaling by M_{eq}^E. That is, $IM_{eq}^E\ (r/D_{eq} * 50)^2$ is plotted in Fig. 6, I being the measured intensity. The exponent E is taken to be -8.5 and -7.5 at $\theta = 25$ deg and 90 deg, respectively. The rationale was touched upon in Sec. II. More specifically, the amplitude of the spectra scaled with exponents -8.5 and -6.5 at $\theta = 25$ deg and 90 deg, respectively. The frequency, on the other hand, scaled with the ambient speed of sound (Helmholtz number scaling) and jet velocity (Strouhal number scaling) at $\theta = 25$ deg and 90 deg, respectively [12]. This led to the choice of the exponents for normalization of I.

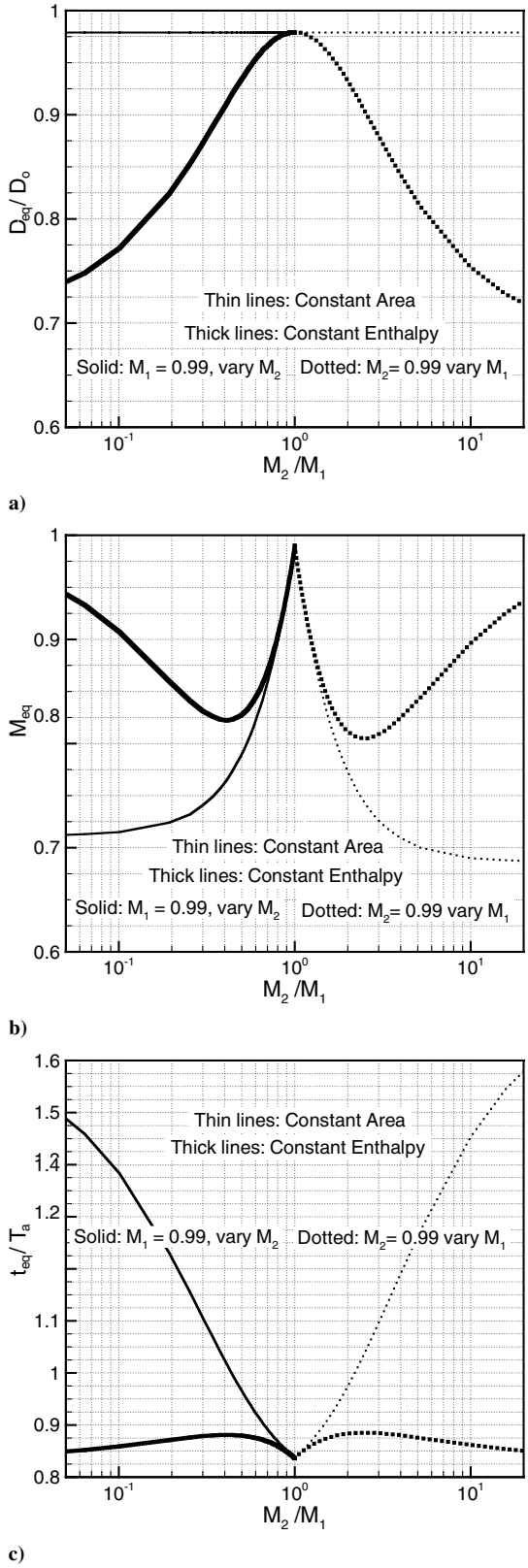

Fig. 4 Equivalent single jet parameters versus R; a) diameter, b) Mach number, and c) temperature.

The apparently disparate sets of data of Fig. 5a have collapsed quite well in Fig. 6a. The single jet from the inner nozzle is represented at $R = 0$ (shown arbitrarily at $R = 0.08$ to fit in the log scale). The condition $R = 1$ also represents a single jet except for the effect of the thin lip of the inner nozzle. Before commenting on the amplitudes at other values of R, we note that the normalized intensity is somewhat lower at $R = 1$ than that at $R = 0$. The reason for this

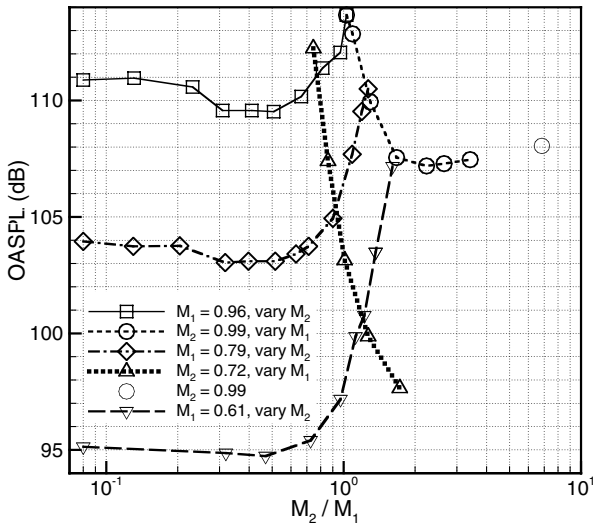

a)

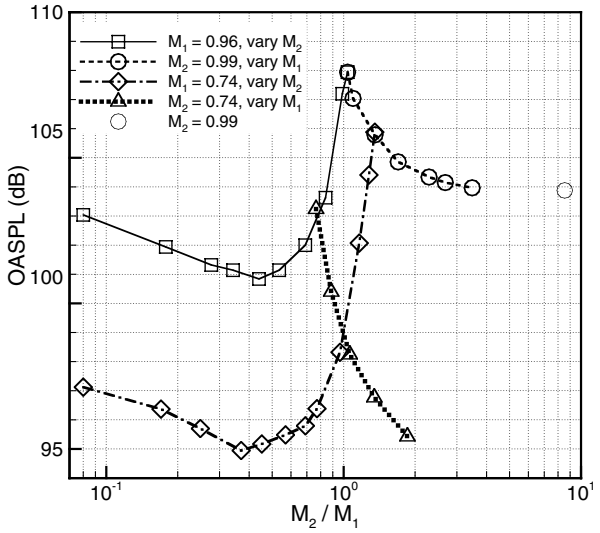

b)

Fig. 5 Overall sound pressure level (OASPL) versus Mach number ratio R for indicated run conditions; a) $\theta = 25$ deg; b) $\theta = 90$ deg; all data referenced to $r/D_1 = 50$.

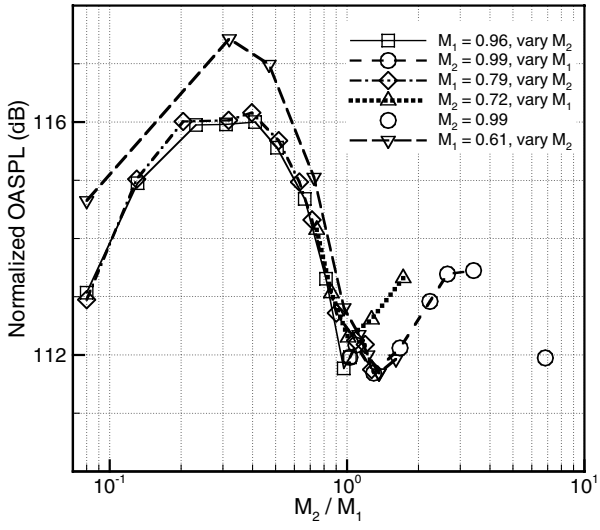

a)

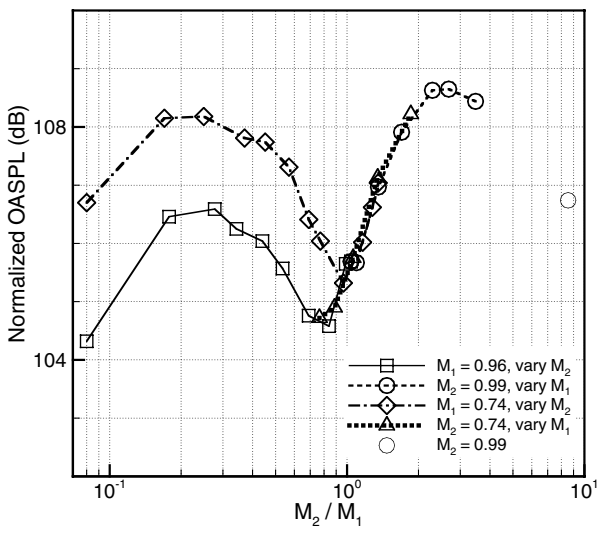

b)

Fig. 6 OASPL data of Fig. 5 normalized by equivalent jet parameters (constant enthalpy); a) $\theta = 25$ deg; b) $\theta = 90$ deg; data referenced to $r/D_{\text{eq}} = 50$.

might be the data scatter discussed in connection with Fig. 2. Here, the difference is about 1.5 dB for most of the data which is within the observed scatter. This could arise from differences in the upstream geometry of the nozzles. The contraction ratio and contours for the inner and outer nozzles are different; recall the nozzle geometry effect observed in [11]. Nevertheless, the trend in the R range of 0–1 (normal velocity profile) is unambiguous. There, as inferred by Tanna [4], the coannular jet is noisier. A similar observation is made from the data at $\theta = 90$ deg (Fig. 6b) for this R range.

It should be noted that in most previous studies noise comparison was made in a somewhat different manner. Typically, the measured intensity was plotted versus velocity ratio and another curve was plotted to represent the expected intensity for the SEJ. The latter curve was obtained by calculating the SEJ at each operating point and predicting its noise from available correlations (e.g., SAE code used in [9]). The difference between the two curves indicated noise increase or decrease. Here, we chose to present the data simply after normalization by the SEJ parameters. The noise intensity of the SEJ is represented at $R = 0$ or $R = 1$. Comparison with the level at either R identifies the increase or decrease in the noise. This is a direct comparison without need for others' data or prediction code. Also, this way the impact of data scatter in the comparison is kept in perspective.

The normalized intensities in both Figs. 6a and 6b are also found to be generally high for $R > 1$ (inverted velocity profile). It reaches a maximum in the R range of 2–3. The present data are in apparent contrast with earlier inferences that inverted velocity profile (IVP) jets are quieter under certain conditions [4,5,9]. This is further examined in Fig. 7. The $\theta = 25$ deg data are normalized by equivalent jet parameters using the constant area procedure and plotted as a function of the velocity ratio, as done in [4]. Note that U_2/U_1 is not significantly different from R at these subsonic conditions; thus, for brevity, we will continue to use the notation R to describe the abscissa of Fig. 7. In Fig. 7a, the full set of data corresponding to Fig. 6a is shown with logarithmic abscissa. First, we note that the normalized amplitude reaches a maximum at $R = 0$. It also continues to increase as R increases on the right-hand side. The increasing levels with $R \to 0$ and $R \to \infty$ follow from the M_{eq}^E scaling and the fact that M_{eq} keeps on decreasing in both limits (Fig. 4b). This underscores the intrinsic flaw with the constant area procedure. The normalized intensities of a single equivalent jet at $R = 0$, 1, or ∞ are predicted different, whereas ideally they should be the same. Here, only at $R = 1$ the energy balance is also satisfied. Thus, a meaningful comparison can only be made with the SEJ at $R = 1$.

For some of the curves in Fig. 7a the level continues to drop past $R = 1$, as R increases. This is further examined by zooming in near

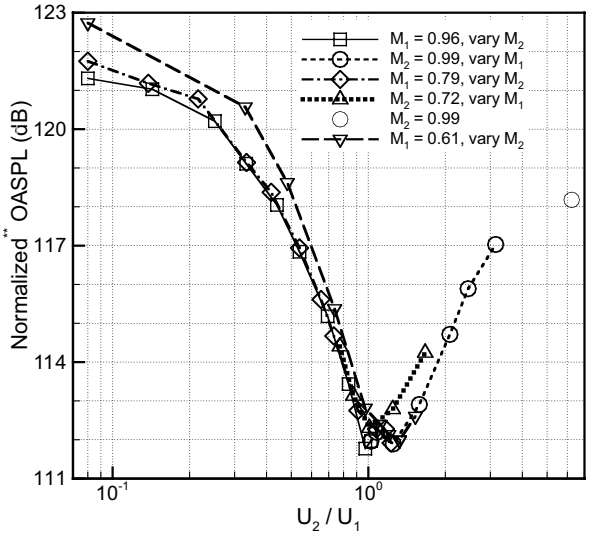

a)

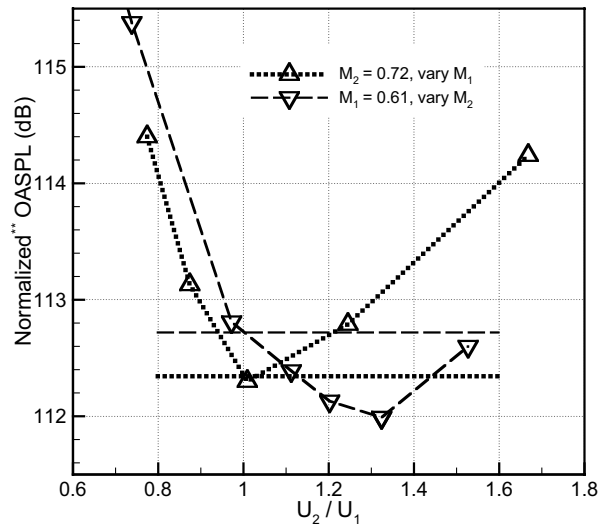

b)

Fig. 7 Normalized OASPL ($\theta = 25$ deg) versus velocity ratio; data referenced to $r/D_{eq} = 50$. (Equivalent jet parameters based on constant area.)**

$R = 1$, in Fig. 7b. For clarity only two cases are shown. We recall that noise reduction was inferred in [4,5,9] for the approximate R range of 1–2. This is borne out by the case shown by the dashed curve with the inverted triangular symbols. For comparison a dashed horizontal line is drawn through the level at $R = 1$. Lower intensity is observed approximately over $1 < R < 1.5$. The decrease, relative to the intensity at $R = 1$, is less than a dB. On the other hand, for three out of five cases of Fig. 7a, for example, the one shown by the dotted line in Fig. 7b, the level is the lowest at $R = 1$. Thus, the present nozzle and run conditions do not affirm a clear noise suppression with the IVP jets. Note that this observation is not contingent upon the procedure for obtaining the SEJ; the same trends exist in the data shown in Fig. 6a. Note furthermore from Fig. 6b that none of the cases at $\theta = 90$ deg exhibit lower noise for $R > 1$.

Returning to the dashed curve of Fig. 7b, one notes that the fraction of a dB noise reduction at $R \approx 1.3$ is within the scatter band discussed in connection with Fig. 2. However, the observed reduction is real and repeatable since the data pertain to the same experimental run in the same facility. It is noted that the two sets of curves in Fig. 7b intersect at a point where M_2 and M_1 are approximately 0.72 and 0.61, respectively. This attests to good data repeatability. When the operating point with this Mach number pair is reached, the same intensity is measured in the two different runs. At $R \approx 1.3$, the Mach number pair (M_2, M_1) for the dashed and the dotted curves are (0.79, 0.61) and (0.72, 0.56), respectively. Thus, noise reduction has occurred at relatively higher Mach numbers. However, at even higher values (0.99, 0.76), corresponding to the circular data points in Fig. 7a, the intensity is again the lowest at $R \approx 1$. One may speculate that factors such as internal noise or the effect of the inner nozzle lip thickness might have led to these ambiguous results for the IVP jets. The influence of these factors is likely to be facility dependent and may also vary with varying run condition with a given facility. It should be noted that while moderate noise reduction was observed with unheated IVP jets, the reduction was found to be more pronounced when the velocity ratio was effected by temperature rather than the driving pressures (i.e., for heated jets) [15]. The issue of noise reduction with unheated IVP jets has basically remained unclear. Overall, for the conditions of the present experiment, it is fair to say that a single jet with top-hat velocity profile is the quietest and nonuniformities introduced by the coannular configuration lead to higher noise.

B. Spectral Data

The measured spectra are presented in Fig. 8 for $\theta = 25$ deg. For clarity, data for $R < 1$ and $R > 1$ are shown separately in Figs. 8a and 8b , respectively. Recall that the overall intensity first decreases with increasing R reaching a minimum around $R = 0.5$ (Fig. 5a). The spectra in Fig. 8a reveal that the energy at low frequencies actually

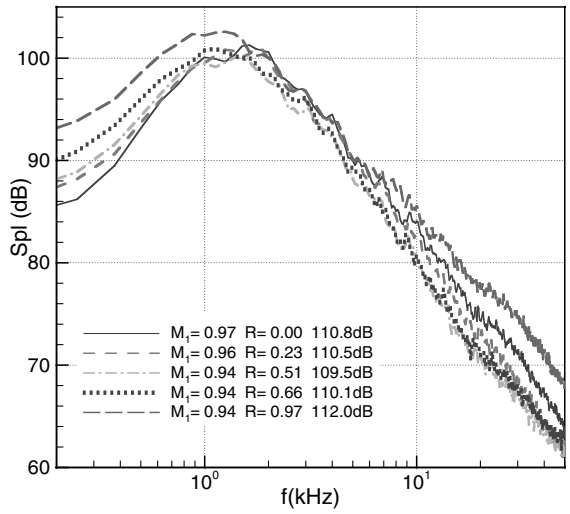

a)

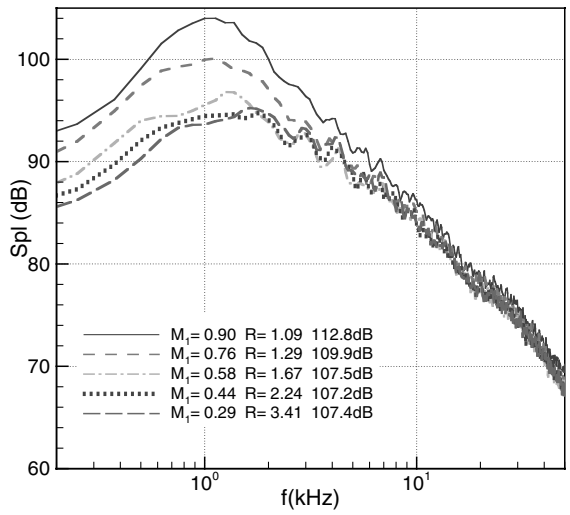

b)

Fig. 8 Sound pressure level spectra at $\theta = 25$ deg. a) $M_1 \approx 0.95$, R varying in the range 0–1; b) $M_2 \approx 0.99$, R varying in the range 1–3.5.

increases at first with increasing R; the decrease in overall intensity comes from a reduction of energy near the peak and high frequencies. At $R \approx 1$ the amplitudes are larger over the entire bandwidth. In Fig. 8b, all the traces on the high-frequency end are conspicuously congruent. This suggests that the high-frequency noise for these (IVP) cases, with fixed M_2, traces to the outer shear layer that remains invariant. A similar observation in [6] led to the assumption of different SEJ parameters for different flow regions, as discussed shortly. Increasing M_1 (decreasing R) in Fig. 8b progressively increases the low-frequency energy. A continual decrease in the frequency of the peak with decreasing R is also observed. Corresponding data for $\theta = 90$ deg are shown in Figs. 9a and 9b, and essentially similar observations can be made.

The spectral data of Figs. 8 and 9 are plotted in Figs. 10 and 11, respectively, in the format of Fig. 2; D_{eq} and M_{eq} are used for the normalization. It can be seen in Fig. 10a that the levels are the lowest for $R = 0$ and 0.97 (single jet cases). The amplitudes are high over the entire bandwidth at intermediate values of R, consistent with high intensities observed in Fig. 6a. For $R > 1$ in Fig. 10b, the traces on the low-frequency end have now collapsed, at the "expense" of dispersion of the curves at higher frequencies that were congruent in Fig. 8b. In particular, for the IVP cases, it is as if the outermost shear layer determines the high-frequency energy while the equivalent jet parameters govern the low-frequency energy. This was addressed in the analysis of [6], as discussed next. Again, similar observations can be made from data at $\theta = 90$ deg shown in Figs. 11a and 11b.

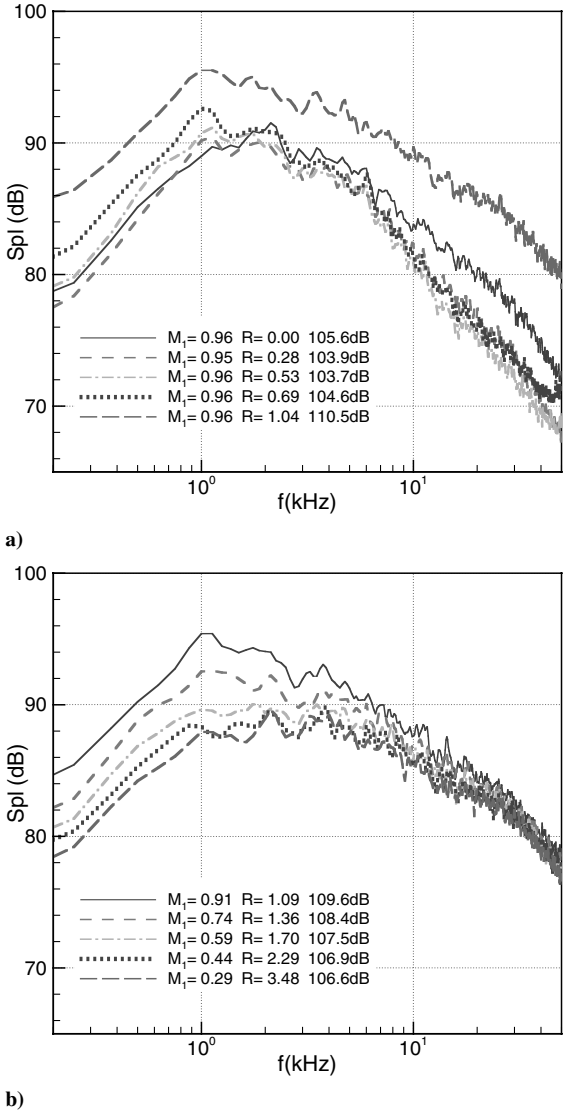

Fig. 9 Sound pressure level spectra at $\theta = 90$ deg. a) $M_1 \approx 0.95$, R varying in the range 0–1; b) $M_2 \approx 0.99$, R varying in the range 1–3.5.

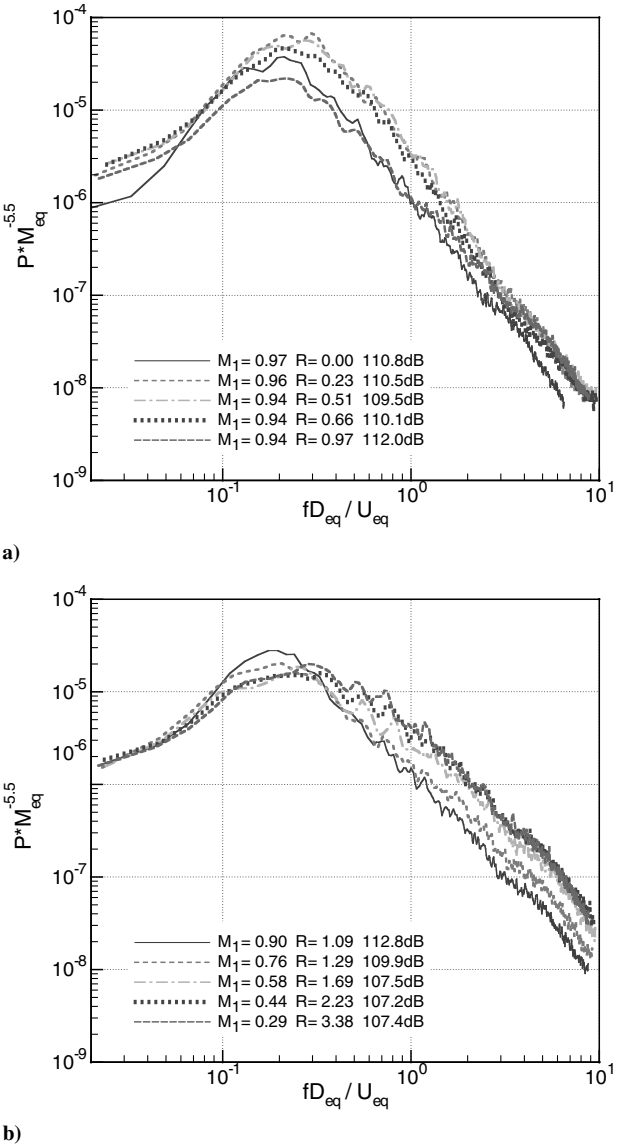

Fig. 10 Sound pressure level spectra of Fig. 8 ($\theta = 25$ deg) normalized by equivalent jet parameters.

The spectral data underscore that it may not be possible to represent the noise from a coannular jet with that of a single equivalent jet. Scaling is different for different noise producing regions of the flow. This was considered earlier in [5] and more thoroughly in [6,7]. Three noise producing regions were identified: 1) an initial mixing layer between the outer stream and the ambient, 2) an interaction region for the primary and secondary mixing layers, and 3) the fully merged region downstream. For region 1, the velocity and length scales were assumed to be the same as the outer stream velocity (U_2) and the outer nozzle diameter (D_o). For region 2, they were assumed to be the primary stream velocity U_1 and a diameter such that the momentum conservation was satisfied. For region 3, enthalpy conservation was also satisfied for heated flows [7], with simplifying assumptions for unheated flows [6]. A prediction scheme synthesizing the noise from the three SEJs (corresponding to the three regions) quite successfully matched the coannular jet noise data. Here, we briefly review the assumptions for obtaining the SEJ parameters in the three regions.

For region 1, the choices of $D_{eq} = D_o$ and $U_{eq} = U_2$ appear appropriate and supported by the congruence of the spectra on the high-frequency end. For region 2, U_1 was taken as U_{eq} while the equivalent diameter was defined as

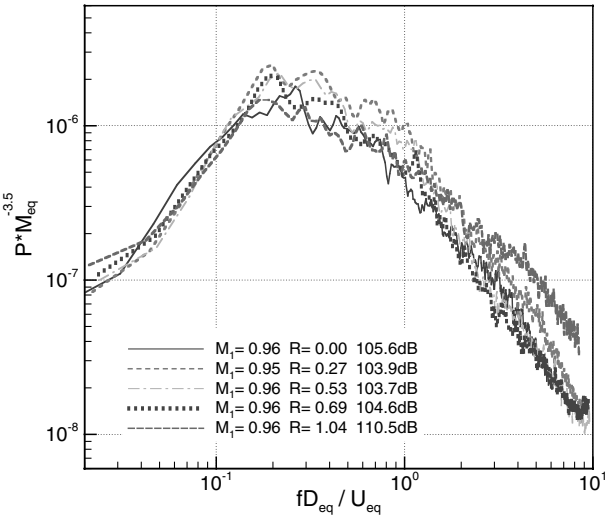

a)

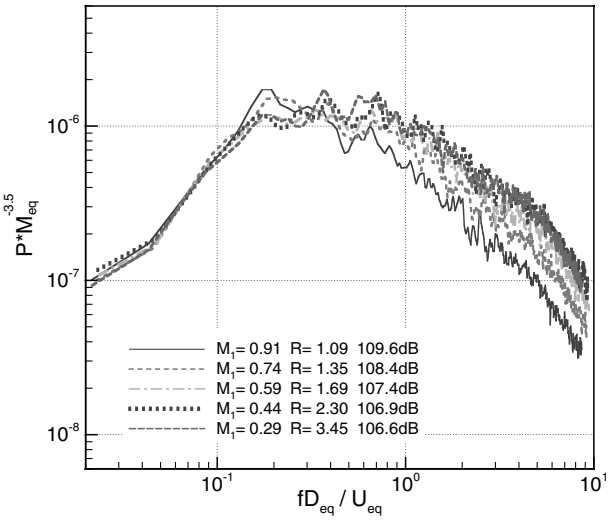

b)

Fig. 11 Sound pressure level spectra of Fig. 9 ($\theta = 90$ deg) normalized by equivalent jet parameters.

$$D_{eq} = D_1(1 + \lambda^2\beta)^{1/2} \tag{11}$$

where $\lambda = U_2/U_1$ and $\beta = \rho_2 A_2/\rho_1 A_1$. In [6], for region 3, the following expressions were obtained with the simplifying assumption, $\rho_{eq} = \rho_1$:

$$U_{eq} = U_1(1 + \lambda^2\beta)/(1 + \lambda\beta) \tag{12}$$

$$D_{eq} = D_1(1 + \lambda\beta)/(1 + \lambda^2\beta)^{1/2} \tag{13}$$

In [7], enthalpy conservation was employed to obtain the following expressions for region 3:

$$U_{eq} = U_1\frac{(1 + \lambda^2\beta'\delta)}{(1 + \lambda\beta'\delta)} \tag{14}$$

and

$$D_{eq} = D_1\left[\frac{(1 + \lambda\beta')(1 + \lambda\beta'\delta)}{(1 + \lambda^2\beta'\delta)}\right]^{1/2} \tag{15}$$

where $\beta' = A_2/A_1$ and $\delta = \rho_2/\rho_1$.

The emphasis in [6] was on jets with normal velocity profiles where Eq. (11) applied well. We note that this definition may not apply for IVP jets, because in the limit $U_1 \to 0$, D_{eq} would be infinity. Derivation of D_{eq} and M_{eq} with Eqs. (12) and (13) yielded results in good agreement with the constant enthalpy (thick line) curves of Fig. 4 for $R < 1$. However, significant differences occurred for $R > 1$. Finally, with regards to Eqs. (14) and (15), it is apparent that conservation of static enthalpy rather than total (stagnation) enthalpy was employed. In the format of Eq. (8) static rather than total temperature was used in [7] for T. Derivation of M_{eq} and D_{eq} with Eqs. (14) and (15) also yielded the same trend as seen in Figs. 4a and 4b (thick line curves); the amplitudes differed only slightly. Obviously, the differences did not pose a problem in the noise synthesis and could be absorbed in the correlation coefficients. However, it would be more rational to use the stagnation enthalpy conservation equation for region 3 and, perhaps, also for region 2.

C. Centerline Mach Number Data

Centerline data were obtained by pitot-static probe surveys. Variations of static pressure for selected cases are shown in Fig. 12. The data exhibit subambient pressures over a large range of axial distance. This phenomenon for single jets has been addressed in prior publications [16,17]. An increase in momentum flux, following regions of high turbulence intensities, is balanced by a drop in the static pressure. It is also seen that most of the cases start with a positive pressure near the nozzle that at first increases before dropping to negative values. At large R a negative pressure is encountered at the exit. As stated before, the limiting case of $R = \infty$ has been excluded because the noise appeared abnormally high. This case was also marked by much lower negative pressures near the exit possibly due to a recirculation bubble occurring over the inner region.

The static and pitot pressures yielded the Mach number profiles. These are shown in Fig. 13a for several cases. For $R < 1$, a lengthening of the potential core can be noticed with increasing R [18]. For $R > 1$, a peak occurs around $x/D_o = 5$, due to the fact that it takes some distance before the higher momentum annular flow gets mixed with the inner flow. The inverse of Mach number, normalized by the SEJ parameters, is plotted in Fig. 13b. We note that for $R = 0$ and 0.99 (two solid curves) the results are close to each other, as expected, because each represents the single jet. For $R < 1$ the curves are shifted downstream, the maximum shift occurring at $R = 0.5$. This shift appears to be simply due to the fact that M_{eq}/M starts with a value smaller than unity. For $R > 1$, the curves are shifted upstream. Here, M_{eq}/M at first decreases to a minimum before increasing. The lowest value before the start of the increase is greater than unity causing the upstream shift of the curves.

The characteristics of the Mach number profiles are further analyzed in Figs. 14 and 15. The asymptotic slope is shown by the diamond symbols in Fig. 14. It is found to be about 0.14, close to but somewhat less than the value (0.16) noted in [19] for single jets.

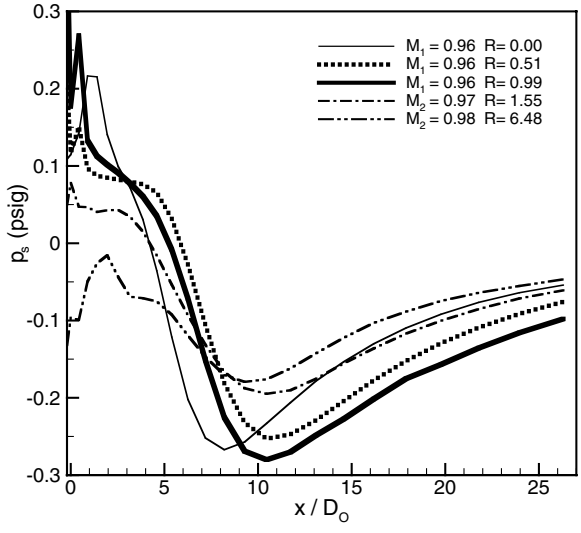

Fig. 12 Centerline variation of static pressure.

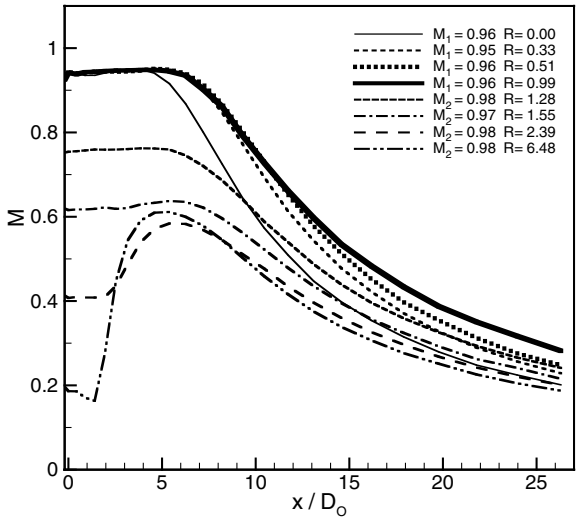

a)

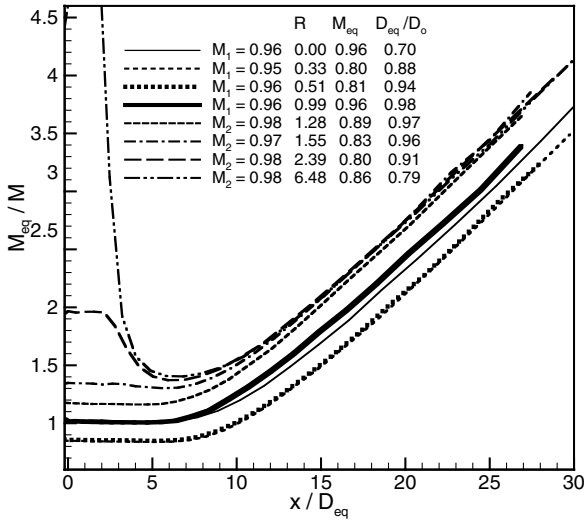

b)

Fig. 13 Centerline variation of Mach number: a) M versus x/D_o; b) same data normalized by equivalent jet parameters.

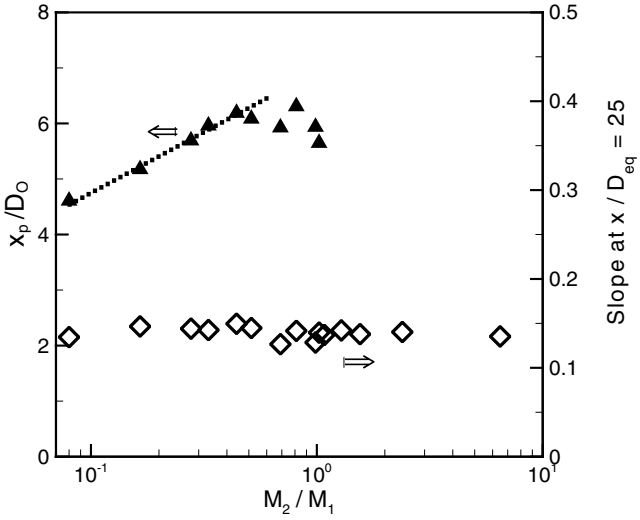

Fig. 14 Asymptotic slope at $x/D_{eq} = 25$ and potential core length (x_p/D_o) from the Mach number curves of Fig. 13.

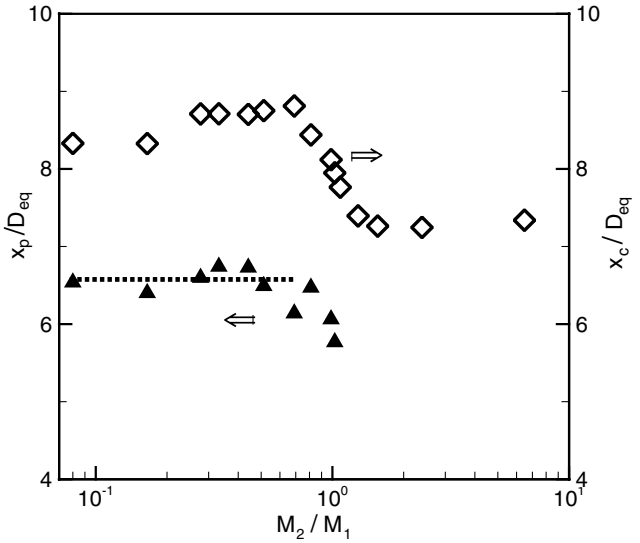

Fig. 15 Potential core length (x_p/D_{eq}) and virtual origin (x_c/D_{eq}) from the Mach number curves of Fig. 13.

"Potential core length" (x_p) is also plotted in Fig. 14. It is defined as the distance from the exit where the Mach number drops to 99% of the initial value. The data are not shown for $R > 1$ since x_p is ill defined in that regime. An increase in x_p with increasing R is seen clearly in Fig. 14. The upstream shift of the Mach number curves in Fig. 13b is reflected in a decrease of x_p across $R = 1$.

The potential core length data normalized by D_{eq} are shown in Fig. 15. For $R < 1$, x_p/D_{eq} turns out to be approximately constant at 6.5. This value is comparable to that found for single jets at high subsonic conditions [19]. It is also noteworthy that in [18] x_p/D_{eq} data were presented for coannular jets with fully expanded inner stream at $M_1 = 1.5$, for two bypass ratios. D_{eq} was defined simply based on conservation of the mass-flow rate. A length $x_p/D_{eq} \approx 7$ was inferred for both cases that is comparable to the present data.

Finally, the lateral shift of the M curves of Fig. 13b is clearly captured by the "virtual origin" (x_c) data shown by the diamond symbols in Fig. 15. It is defined the same way as in [19] and represents the distance of the intersection of the $M_{eq}/M = 1$ line with a radial line from the origin to a data point in the asymptotic region (taken at $x/D_{eq} = 25$). The abrupt shift across $R = 1$ is clearly seen. The approximate value of $x_c/D_{eq} = 8$ at both $R = 0$ and 1 agrees with the equation,

$$x_c/D_{eq} = 7.0 + 1.2M_{eq}^2 + 1.2(1 - t_{eq}/T_a) \qquad (16)$$

cited in [19]. Overall, except for the virtual origin shift, the characteristics of the centerline Mach number decay agree well with single jet characteristics analyzed in [19].

V. Conclusions

Far-field noise and centerline Mach number decay data are documented in this paper for subsonic coannular jets. Scaling of the data is considered based on single equivalent jet parameters calculated by satisfying continuity, momentum, and energy equations. The results confirm that coannular jets with "normal" velocity profiles are noisier than the single equivalent jet. Jets with inverted velocity profiles are also found to be noisier except in a narrow range around $R = 1.3$. In the latter range a few data sets display noise reduction relative to the level at $R = 1$. But several other data sets exhibit higher noise for the entire IVP range ($R > 1$). The issue of noise reduction with the IVP jets has remained unclear. Overall, for the parametric ranges covered in the present experiment, a single jet with top-hat velocity profile is found to be the quietest. Any nonuniformity introduced by the coannular configuration leads to higher noise. When normalized by equivalent jet parameters the asymptotic Mach number decay rates, as well as potential core lengths, are found to be comparable to those of a single jet. However,

discontinuities are observed around $R = 1$. Specifically, an abrupt shift in the virtual origin is noted across this boundary.

Acknowledgments

Support from the Quiet Aircraft Technology and Subsonic Fixed Wing Programs during the course of this study is gratefully acknowledged.

References

[1] Papamoschou, D., and Debiasi, M., "Conceptual Development of Quiet Turbofan Engines for Supersonic Aircraft," *Journal of Propulsion and Power*, Vol. 19, No. 2, 2003, pp. 161–169.

[2] Zaman, K. B. M. Q., "Noise- and Flow-Field of Jets from an Eccentric Coannular Nozzle," AIAA Paper 2004-0005, Jan. 2004.

[3] Williams, T. J., Ali, M. R. M. H., and Anderson, J. S., "Noise and Flow Characteristics of Coaxial Jets," *Journal of Mechanical Engineering Science*, Vol. 11, No. 2, 1969, pp. 133–142.

[4] Tanna, H. K., "Coannular Jets—Are They Really Quiet and Why?," *Journal of Sound and Vibration*, Vol. 72, No. 1, 1980, pp. 97–118.

[5] Tanna, H. K., and Morris, P. J., "The Noise from Normal-Velocity-Profile Coannular Jets," *Journal of Sound and Vibration*, Vol. 98, No. 2, 1985, pp. 213–234.

[6] Fisher, M. J., Preston, G. A., and Bryce, W. D., "A Modeling of the Noise from Simple Coaxial Jets, Part 1: With Unheated Primary Flow," *Journal of Sound and Vibration*, Vol. 209, No. 3, 1998, pp. 385–403.

[7] Fisher, M. J., Preston, G. A., and Mead, C. J., "A Modeling of the Noise from Simple Coaxial Jets, Part 2: With Heated Primary Flow," *Journal of Sound and Vibration*, Vol. 209, No. 3, 1998, pp. 405–417.

[8] Ko, N. W. M., and Kwan, A. S. H., "The Initial Region of Subsonic Co-Axial Jets," *Journal of Fluid Mechanics*, Vol. 73, No. 2, 1976, pp. 305–332.

[9] Pao, S. P., "A Correlation of Mixing Noise from Coannular Jets with Inverted Flow Profiles," NASA TP 1301, April 1979.

[10] Bridges, J. E., and Brown, C. A., "Validation of the Small Hot Jet Acoustic Rig for Jet Noise Research," AIAA Paper 2005-2846, 23–25 May 2005.

[11] Viswanathan, K., and Clark, L., "Effect of Nozzle Internal Contour on Jet Aeroacoustics," AIAA Paper 2004-0008, Jan. 2004.

[12] Zaman, K. B. M. Q., and Yu, J. C., "Power Spectral Density of Subsonic Jet Noise," *Journal of Sound and Vibration*, Vol. 98, No. 4, 1985, pp. 519–537.

[13] Bass, H. E., Sutherland, L. C., Zuckerwar, A. J., Blackstock, D. T., and Hester, D. M., "Atmospheric Absorption of Sound: Further Developments," *Journal of the Acoustical Society of America*, Vol. 97, No. 1, 1995, pp. 680–683.

[14] Zaman, K. B. M. Q., "Effect of Initial Condition on Subsonic Jet Noise," *AIAA Journal*, Vol. 23, No. 9, 1985, pp. 1370–1373.

[15] Maus, J. R., Goethert, B. H., and Sundaram, C. V., "Noise Characteristics of Coannular Flows with Conventional and Inverted Velocity Profiles," AIAA Paper 80-0167, Jan. 1980.

[16] Hussain, A. K. M. F., and Clark, A. R., "Upstream Influence on the Near Field of a Plane Turbulent Jet," *Physics of Fluids*, Vol. 20, 1977, pp. 1416–1426.

[17] Zaman, K. B. M. Q., "Flow Field and Near and Far Sound Field of a Subsonic Jet," *Journal of Sound and Vibration*, Vol. 106, No. 1, 1986, pp. 1–16.

[18] Murakami, E., and Papamoschou, D., "Mean Flow Development in Dual-Stream Compressible Jets," *AIAA Journal*, Vol. 40, No. 6, 2002, pp. 1131–1138.

[19] Zaman, K. B. M. Q., "Asymptotic Spreading Rate of Initially Compressible Jets—Experiment and Analysis," *Physics of Fluids*, Vol. 10, No. 10, 1998, pp. 2652–2660.

C. Bailly
Associate Editor